PERGAMON

International Journal of Heat and Mass Transfer 45 (2002) 1379–1391

International Journal of HEAT and MASS TRANSFER

www.elsevier.com/locate/ijhmt

Nonlinear analysis of tilted toroidal thermosyphon models

Arturo Pacheco-Vega [a], Walfre Franco [a], Hsueh-Chia Chang [b], Mihir Sen [a,*]

[a] *Department of Aerospace and Mechanical Engineering, University of Notre Dame, Notre Dame, IN 46556-5637, USA*
[b] *Department of Chemical Engineering, University of Notre Dame, Notre Dame, IN 46556, USA*

Received 27 December 2000; received in revised form 10 August 2001

Abstract

We analyze one-dimensional models for single-phase tilted toroidal thermosyphons for three different heating conditions: *known heat flux*, *known wall temperature* and *mixed heating*. For the first two the governing equations lend themselves to exact reduction to a set of three ordinary differential equations, while for the third the equations remain coupled as an infinite set. For all three cases, the tilt angle is stabilizing while the heat rate is a destabilizer. A nonlinear analysis is carried out using center manifold theory and normal form analysis. The known heat flux solutions lose stability through a supercritical Hopf bifurcation, while for the other two heating conditions the Hopf bifurcation is supercritical under some conditions and subcritical under others. Stable limit-cycle oscillations exist only for the supercritical cases, otherwise instability leads directly to chaos. Analysis also provides an estimate for the amplitude of oscillation for the supercritical conditions. Numerical experiments have confirmed the theoretical predictions qualitatively and quantitatively.

1. Introduction

Single-phase natural convective loops or thermosyphons are used in a variety of engineering applications, such as nuclear reactor cooling, solar collectors, etc. [1–4]. They have also been studied because they provide an excellent theoretical introduction to convection in more complex geometries. Experiments have been carried out with toroidal [5–7] and rectangular [8] loops. Of these [6] and [8] worked with variable loop inclinations. Most analytical models are one-dimensional in the sense that the fluid velocity and temperature are averaged over a cross-section. These models have been especially significant since it has been found that, for certain geometries and under certain thermal conditions, the governing equations can be reduced to a set of three ordinary differential equations that can exhibit chaotic behavior [9–11].

Due to the variety of geometries that can be used and thermal conditions that can be applied, comparison between theory and experiment is approximate unless the same conditions are considered for both. It is sometimes assumed that all thermal conditions and loop geometries give similar results; this may perhaps be true for overall qualitative behavior, but certainly not in the details. The occurrence of chaos in these mathematical models has been an aspect that has attracted the attention of many researchers, and certainly all of them, under specific conditions, do that.

The focus on chaos has obscured the fact that the geometry and heating condition significantly affect the details of system behavior and there is some confusion in the literature in this regard. For example, some experiments [5,8] have shown the presence of stable oscillations while the most commonly used model based on the Lorenz equations does not show the existence of stable limit cycles [9]. The existence or not of oscillations is important for the design of convection loops in actual applications. In this work we will clarify the situation by choosing the simplest geometry possible, the torus, and apply the commonly used heating conditions. In each case, we will be interested in the effect of nondimensional parameters corresponding to heating and tilt angle.

Each of the heating conditions will be examined separately though in a very similar manner. The steady states will be found and their linear stability determined.

* Corresponding author. Tel.: +1-219-631-5975; fax: +1-219-631-8341.
E-mail address: mihir.sen.1@nd.edu (M. Sen).

0017-9310/02/$ - see front matter
PII: S0017-9310(01)00265-4

Nomenclature

c	specific heat of fluid at constant pressure
d	tube diameter
f	friction coefficient $= 8\mu/d$ for fully developed flow
g	acceleration due to gravity
h	heat transfer coefficient
H	nondimensional heat transfer coefficient
q	heat rate per unit length
$\widehat{q}$	amplitude of heat flux variation
Q	nondimensional heat flux
r	radial coordinate, amplitude of limit cycle
R	torus radius
s	longitudinal coordinate
t	time
T	fluid temperature
T_c	uniform wall temperature distribution
T_m^c	Fourier cosine coefficient of temperature
T_m^s	Fourier sine coefficient of temperature
T_w	wall temperature
$\widehat{\delta T}$	amplitude of temperature variation
ΔT	nondimensional amplitude of temperature variation
u	average fluid velocity
x	nondimensional fluid velocity
y_m	nondimensional Fourier cosine coefficient of temperature
z_m	nondimensional Fourier sine coefficient of temperature

Greek symbols

α	tilt angle
β	coefficient of thermal expansion
δ	linear coefficient in amplitude equation
ϵ	order of perturbation in parameter space
θ	angular coordinate
λ	eigenvalue
μ	dynamic viscosity
ρ	fluid density
σ	nonlinear coefficient in amplitude equation
τ	nondimensional time

Subscripts and superscripts

$-$	time independent solution
cr	critical value

The nature of the loss of stability will be analyzed by center manifold theory and normal form analysis [12], a method that allows the determination of system behavior near a bifurcation point by means of nonlinear changes of coordinates that reduce the dimension of the problem. The center manifold is an invariant manifold in phase space from which trajectories will not escape; it is tangent to the eigenspace spanned by the eigenvectors of the Jacobian matrix of the system at the fixed point. The center manifold theorem [12–14] then states that there is a local nonlinear transformation of the dependent variables such that the transformed stable eigenmodes decay exponentially and the nonlinear dynamics are governed only by the equations on the center manifold. We will use the center manifold projection (CMP) technique of Carr [13] to reduce the multi-dimensional system to a two-dimensional time-invariant manifold and derive its coefficients which define the nature of the instability. The analytical results obtained this way will be confirmed by a fourth-order Runge–Kutta numerical simulation.

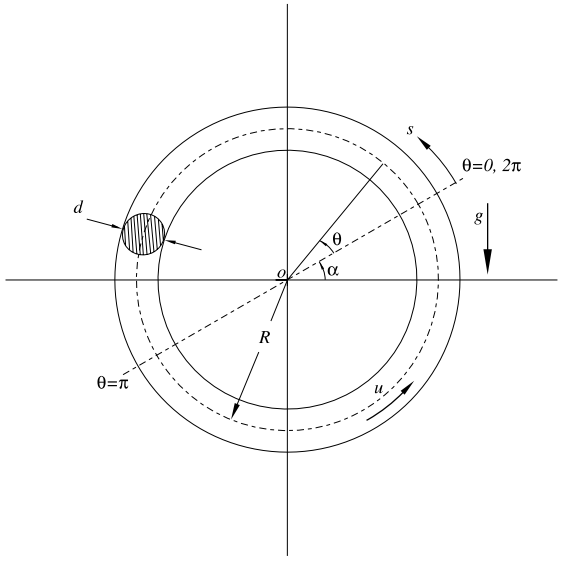

Fig. 1. Schematic of toroidal thermosyphon.

2. Problem description

Consider a fluid-filled loop, shown in Fig. 1, in the form of a torus with tube diameter d and the torus radius R, where $d \ll R$. The loop is heated in some parts and cooled in others. The temperature differences within the fluid lead to changes in density and hence buoyancy forces that create natural circulation. We will use the Boussinesq approximation which neglects change in fluid density in all but the buoyancy force term. The dependent variables are the cross-sectional average of

the fluid velocity u and the temperature T. The independent variables are the time t and the angular coordinate θ which is measured counterclockwise from a line that is inclined at an angle α with respect to the horizontal plane. This line also separates regions with heating and cooling. The angle α will be referred to as the tilt or inclination of the loop since it is varied in experiments by rotating the loop about a horizontal axis normal to its plane.

Due to mass conservation, u is independent of θ and is a function of t alone. The integral of the momentum equation over the loop gives

$$\frac{\mathrm{d}u}{\mathrm{d}t}+\frac{4f}{\rho d}u=\frac{\beta g}{2\pi}\int_0^{2\pi} T\cos(\theta+\alpha)\,\mathrm{d}\theta, \tag{1}$$

where $u=u(t)$ and $T=T(\theta,t)$. The frictional wall shear has been taken to be proportional to the mean fluid velocity with f being the proportionality constant, ρ is the fluid density, β is its coefficient of thermal expansion and g is the acceleration due to gravity. The energy equation is given by

$$\frac{\partial T}{\partial t}+\frac{u}{R}\frac{\partial T}{\partial \theta}=\frac{4q}{\pi d^2\rho c}, \tag{2}$$

where c is the specific heat of the fluid, and q is the heat rate per unit length of the loop. Heat transfer due to axial conduction has been neglected since it is important only for the onset of convection.

Expanding the temperature in a Fourier series as

$$T(\theta,t)=T_0^{\mathrm{c}}(t)+\sum_{m=1}^{\infty}\left[T_m^{\mathrm{c}}(t)\cos m\theta+T_m^{\mathrm{s}}(t)\sin m\theta\right] \tag{3}$$

and substituting in Eq. (1), the momentum equation becomes

$$\frac{\mathrm{d}u}{\mathrm{d}t}+\frac{4f}{\rho d}u=\frac{\beta g}{2}\left(T_1^{\mathrm{c}}\cos\alpha-T_1^{\mathrm{s}}\sin\alpha\right). \tag{4}$$

Nondimensionalization of the governing equations will be carried out using

$$u=\frac{4fR}{\rho d}x,\quad t=\frac{\rho d}{4f}\tau,\quad T_m^{\mathrm{c}}=\frac{32f^2R}{\rho^2d^2\beta g}y_m,\quad T_m^{\mathrm{s}}=\frac{32f^2R}{\rho^2d^2\beta g}z_m, \tag{5}$$

where x and τ are the nondimensional fluid velocity and time, respectively, and y_m and z_m are the nondimensional Fourier coefficients of the temperature.

There are three different cases of heating conditions that will be discussed separately.

(a) *Known heat flux* where $q(\theta)$ is known over the entire loop. This gives a simple mathematical model, but since a prescribed heat extraction is difficult to achieve in practice, this condition has not been experimentally tested.

(b) *Known wall temperature* where the temperature of the wall, $T_{\mathrm{w}}(\theta)$, is known over the loop, and heat transfer to the fluid is by thermal convection. Both analysis and experiments are simple to carry out. The effect of the tilt angle has, however, not been previously reported in detail for this heating condition.

(c) *Mixed heating* where the heat flux is known for part of the loop and the wall temperature is known for the rest. This is the most practical thermal condition from an experimental point of view, since heating can be achieved by electrical heaters and cooling by heat exchangers, and is the one that is perhaps most common in engineering applications. The analysis is complicated by the fact that the governing equations *cannot* be reduced to a finite set of ordinary differential equations except by truncation.

3. Known heat flux

The linear stability analysis and numerical solutions of this problem were reported in Sen et al. [15].

3.1. Dynamical model

The simplest heating condition is when the heat rate per unit length is a sine function, $q(s)=-\widehat{q}\sin\theta$, where the angular θ, and longitudinal s, coordinates are related by the radius of the torus R. Other periodic forms with zero mean value give the same three equations. Locally, a positive q indicates heating, and the negative indicates cooling. Eqs. (2) and (3) give

$$\frac{\mathrm{d}T_0^{\mathrm{c}}}{\mathrm{d}t}+\sum_{m=1}^{\infty}\left(\frac{\mathrm{d}T_m^{\mathrm{c}}}{\mathrm{d}t}\cos m\theta+\frac{\mathrm{d}T_m^{\mathrm{s}}}{\mathrm{d}t}\sin m\theta\right)+\frac{u}{R}\sum_{m=1}^{\infty}\left(-mT_m^{\mathrm{c}}\sin m\theta+mT_m^{\mathrm{s}}\cos m\theta\right)=-\frac{4\widehat{q}}{\pi d^2\rho c}\sin\theta. \tag{6}$$

Integrating around the loop, we obtain $\mathrm{d}T_0^{\mathrm{c}}/\mathrm{d}t=0$ from which we find that T_0^{c} is a constant. Also on multiplying Eq. (6) first by $\cos\theta$ and integrating from 0 to 2π, and then repeating the procedure with $\sin\theta$, we get the pair of equations:

$$\frac{\mathrm{d}T_1^{\mathrm{c}}}{\mathrm{d}t}+\frac{u}{R}T_1^{\mathrm{s}}=0, \tag{7}$$

$$\frac{\mathrm{d}T_1^{\mathrm{s}}}{\mathrm{d}t}-\frac{u}{R}T_1^{\mathrm{c}}=-\frac{4\widehat{q}}{\pi d^2\rho c}. \tag{8}$$

The nondimensional form of the governing equations (4), (7) and (8) is

$$\frac{\mathrm{d}x}{\mathrm{d}\tau}=-x+y\cos\alpha-z\sin\alpha, \tag{9}$$

$$\frac{\mathrm{d}y}{\mathrm{d}\tau}=-xz, \tag{10}$$

$$\frac{dz}{d\tau} = -Q + xy, \tag{11}$$

where we have dropped the subscript 1 from y_1 and z_1. The governing parameters are

$$Q = \frac{\widehat{q}\rho^2 d\beta g}{32\pi c f^3 R} \tag{12}$$

representing the magnitude of the heating, and α, which is the tilt of the loop.

3.2. Steady states and linear analysis

The two critical points of the dynamical system (9)–(11) are $P^+ = (\overline{x}, \overline{y}, \overline{z}) = (\sqrt{Q\cos\alpha},\ \sqrt{Q/\cos\alpha}, 0)$ and $P^- = (\overline{x}, \overline{y}, \overline{z}) = (-\sqrt{Q\cos\alpha}, -\sqrt{Q/\cos\alpha}, 0)$, both of which exist if $-90° < \alpha < 90°$. Here $\overline{x}$, $\overline{y}$, and $\overline{z}$ denote the time independent solutions of the system. A linear stability analysis shows that P^+ is stable as long as $Q \leqslant \sin^2\alpha/\cos^3\alpha$ with $\alpha \geqslant 0$ and unstable otherwise. The eigenvalues at the neutral stability curve $Q = \sin^2\alpha/\cos^3\alpha$, shown in Fig. 2, are -1 and $\pm i\sqrt{2Q\cos\alpha}$ indicating a Hopf bifurcation. It can be observed that the unstable region decreases as the tilt angle is increased. Similarly, P^- is stable for $Q \leqslant \sin^2\alpha/\cos^3\alpha$ and $\alpha \leqslant 0$, and unstable otherwise.

3.3. Nonlinear analysis

Details of the nonlinear analysis are in Appendix A, and we provide only the final results. Just above the neutral stability curve, the system (9)–(11) in polar coordinates (r, θ) is approximated by a Stuart–Landau amplitude and phase equations as

$$\frac{dr}{dt} = \delta(\epsilon) r + \sigma r^3, \quad \frac{d\theta}{dt} = \sqrt{2}\tan\alpha, \tag{13}$$

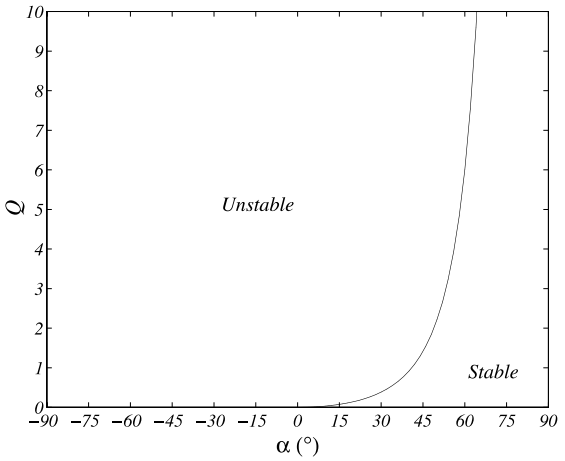

Fig. 2. Known heat flux: neutral stability curve for P^+ in (Q, α) space.

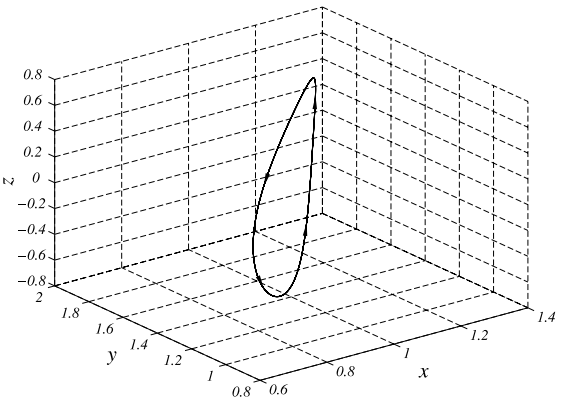

Fig. 3. Known heat flux: attractor in phase space; $\alpha = 45°$, $\epsilon = 0.05$.

where the coefficients of the linear and nonlinear terms in (13) are given explicitly by

$$\delta(\epsilon) = -\frac{\epsilon\sin^2\alpha}{4(\cos^2\alpha - 2)},$$
$$\sigma = -\frac{1}{32}\frac{\sin^2\alpha\cos^2\alpha(\cos^2\alpha - 10/7)}{7\cos^6\alpha - 36\cos^4\alpha + 60\cos^2\alpha - 32} \tag{14}$$

for $0 \leqslant \alpha < 90°$ and $\epsilon > 0$. Here ϵQ_{cr} is a perturbation above the neutral stability curve where $Q_{cr} = \sin^2\alpha/\cos^3\alpha$ is the critical value of the heating parameter. $\delta(\epsilon)$ is always positive while σ is always negative indicating that, along the neutral curve, the Hopf bifurcation is always supercritical and a stable limit cycle is expected in the unstable side. The angular velocity of these periodic oscillations is $\sqrt{2}\tan\alpha$ and the amplitude is $r(\epsilon) = \sqrt{|-\delta(\epsilon)/\sigma|}$. The amplitude $r(\epsilon)$ increases with the heating parameter Q.

For numerical simulation we assume $\alpha = 45°$ and $\epsilon = 0.05$, corresponding to a point in the unstable region just above the neutral curve. The initial transients are discarded. The three-dimensional phase space trajectory is shown in Fig. 3 indicating a stable limit cycle for almost all initial conditions. Similar behavior was obtained at other places along the neutral stability curve confirming the prediction of the CMP theory. Fig. 12 shows a comparison between the analytical and numerical amplitudes for various values of ϵ. The qualitative and quantitative agreement are remarkably good with rms errors of the order of 1%.

4. Known wall temperature

This case was first investigated by Yorke and Yorke [9].

4.1. Dynamical model

We will assume that the wall temperature is given by a sinusoidal variation $T_w = T_c - \widehat{\delta T}\sin\theta$, so that the heat rate per unit length is given by

$$q = \pi d h (T_w - T), \tag{15}$$

where h is a heat transfer coefficient. After substituting the above and Eq. (3) in Eq. (2), the energy equation becomes

$$\begin{aligned}\frac{dT_0^c}{dt} &+ \sum_{m=1}^{\infty}\left(\frac{dT_m^c}{dt}\cos m\theta + \frac{dT_m^s}{dt}\sin m\theta\right)\\ &+ \frac{u}{R}\sum_{m=1}^{\infty}\left(-mT_m^c\sin m\theta + mT_m^s\cos m\theta\right)\\ &= \frac{4h}{d\rho c}\left[T_c - \widehat{\delta T}\sin\theta - T_0^c\right.\\ &\left. - \sum_{m=1}^{\infty}\left(T_m^c\cos m\theta + T_m^s\sin m\theta\right)\right].\end{aligned} \tag{16}$$

Integrations of Eq. (16) from 0 to 2π, first with weight $\cos\theta$ and then repeating with weight $\sin\theta$, give us the ordinary differential equations

$$\frac{dT_0^c}{dt} = \frac{4h}{d\rho c}\left(T_c - T_0^c\right), \tag{17}$$

$$\frac{dT_1^c}{dt} + \frac{u}{R}T_1^s = -\frac{4h}{d\rho c}T_1^c, \tag{18}$$

$$\frac{dT_1^s}{dt} - \frac{u}{R}T_1^c = -\frac{4h}{d\rho c}\left(\widehat{\delta T} + T_1^s\right). \tag{19}$$

Eq. (17) merely describes the time change of the mean temperature.

The nondimensional versions of Eqs. (4), (18) and (19) are

$$\frac{dx}{d\tau} = -x + y\cos\alpha - z\sin\alpha, \tag{20}$$

$$\frac{dy}{d\tau} = -Hy - xz, \tag{21}$$

$$\frac{dz}{d\tau} = -\Delta T - Hz + xy, \tag{22}$$

where the subscript 1 from y_1 and z_1 have been dropped, and

$$H = \frac{h}{fc}, \quad \Delta T = \frac{h\widehat{\delta T}\rho^2 d^2\beta g}{32 f^3 c R}. \tag{23}$$

The governing parameters H and ΔT are the nondimensional forms of the heat transfer coefficient and the amplitude of the temperature distribution, respectively.

4.2. Steady states and linear stability

The critical points of Eqs. (20)–(22) are given by solutions of the cubic

$$\bar{x}^3 + (H^2 - \Delta T\cos\alpha)\bar{x} - H\Delta T\sin\alpha = 0 \tag{24}$$

along with

$$\bar{y} = \frac{\Delta T\bar{x}}{H^2 + \bar{x}^2}, \quad \bar{z} = -\frac{H\Delta T}{H^2 + \bar{x}^2}. \tag{25}$$

The steady-state velocities, determined from Eq. (24), are shown in Fig. 4 for $H = 0.1$ (which is a realistic value for experimental conditions), and different values of the parameter ΔT. Only one critical point exists in the ranges $-180° < \alpha < -\alpha^*$ and $\alpha^* < \alpha < 180°$, where α^* varies from $\alpha^* = 0°$ when $\Delta T = 0^+$ to $\alpha^* = 90°$ as $\Delta T \to +\infty$. On the other hand, there are three critical points in the $-\alpha^* < \alpha < \alpha^*$ range. We designate as P_1 and P_3 the outer positive and negative branches, respectively, and P_2 the inner branch. The critical points P_1 and P_3 correspond to the counterclockwise and clockwise motions of the flow.

Linear stability analysis of the dynamical system leads to a polynomial equation for the eigenvalues

$$\begin{aligned}\lambda^3 &+ (2H+1)\lambda^2 + \left(\bar{x}^2 + H^2 + 2H + \bar{y}\sin\alpha + \bar{z}\cos\alpha\right)\lambda\\ &+ \bar{x}^2 + (\bar{y}\cos\alpha - \bar{z}\sin\alpha)\bar{x}\\ &+ (\bar{y}\sin\alpha + \bar{z}\cos\alpha)H + H^2 = 0.\end{aligned} \tag{26}$$

For P_1 the eigenspectrum contains one stable real eigenvalue and two complex conjugates which can be either stable or unstable depending on the values of α and ΔT. At neutral stability the leading eigenvalues are purely imaginary indicating the existence of a Hopf bifurcation. Fig. 5 shows the neutral stability curve for P_1 in the parameter space $(\Delta T, \alpha)$. As the tilt angle increases, the flow can handle larger temperature

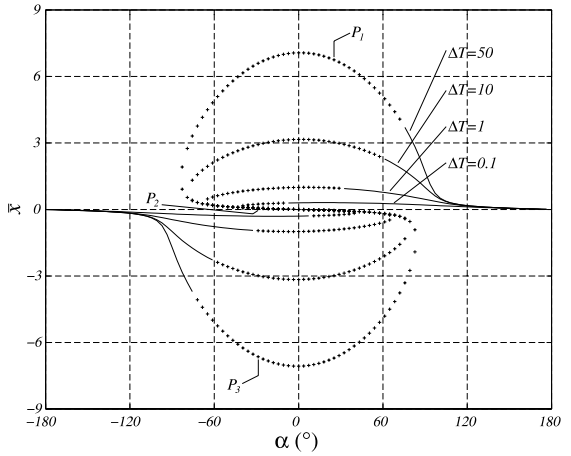

Fig. 4. Known wall temperature: steady-states $\bar{x}(\alpha)$; $H = 0.1$ and different ΔT; − stable; + unstable.

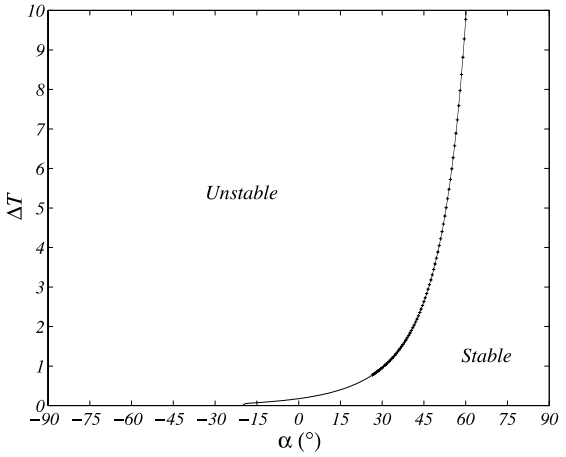

Fig. 5. Known wall temperature: neutral stability curve for P_1 in $(\Delta T, \alpha)$ space; $-$ subcritical; $-+-$ supercritical.

differences before losing stability. The stability curve for P_3 is similar, being a mirror image with respect to the ordinate. P_2 is always unstable [16].

4.3. Nonlinear analysis

A nonlinear analysis similar to that in Appendix A was carried out, though the details will not be presented. Once again we consider a point in the unstable region with $\Delta T = (1+\epsilon)\Delta T_{cr}$, where T_{cr} is the critical value. Stuart–Landau and phase equations similar to Eq. (13) were obtained. The coefficients $\delta(\epsilon)$ and σ cannot be displayed in explicit analytical form but can be calculated from the CMP analysis. The angular velocity, to leading order, is the absolute value of the complex conjugate eigenvalues at the neutral stability curve and hence depends on α.

The results from the CMP analysis show that as we move along the neutral stability curve in Fig. 5, there is a change in the nature of the Hopf bifurcation from sub- to super-criticality that is indicated in the figure. For $\alpha < 26.5°$, σ is positive so that the bifurcation is subcritical, whereas for $\alpha \geqslant 26.5°$ it is negative and solution bifurcates supercritically. Stable limit cycles exist for the supercritical Hopf bifurcation, while for the subcritical part of the curve, chaotic trajectories can be expected to appear as soon as the steady states become unstable.

Numerical integrations of Eqs. (20)–(22) were carried out for $\alpha = 0°$ and $\alpha = 45°$, with $\epsilon = 0.05$. In accordance with the CMP analysis, the numerical solutions for $\alpha = 0°$, shown in Fig. 6(a), give a strange attractor, while the corresponding results for $\alpha = 45°$ shown in Fig. 6(b) produce a limit cycle.

Comparison between the analytical and numerical amplitudes on the unstable side of the supercritical part of the neutral stability curve is shown in Fig. 12. Quantitatively the two solutions diverge slightly with increasing ϵ. This may be due to terms of order ϵ^2 and higher or of order r^5 and higher that were neglected in the nonlinear analysis, since the agreement is good for small ϵ for which both are small. There is complete agreement, however, as to the point of the change from sub- to super-criticality along the Hopf curve since that depends only on the sign of the coefficients of the Stuart–Landau equation.

5. Mixed conditions

This was analyzed by Gorman et al. [7] through a truncated approximation.

5.1. Dynamical model

Here the heating will be through a constant heat flux $\hat{q}$, and the cooling through a constant wall temperature T_c. Thus, we have

$$q = \begin{cases} \pi dh(T_c - T) & \text{for } 0 \leqslant \theta \leqslant \pi, \\ \hat{q} & \text{for } \pi < \theta < 2\pi. \end{cases} \tag{27}$$

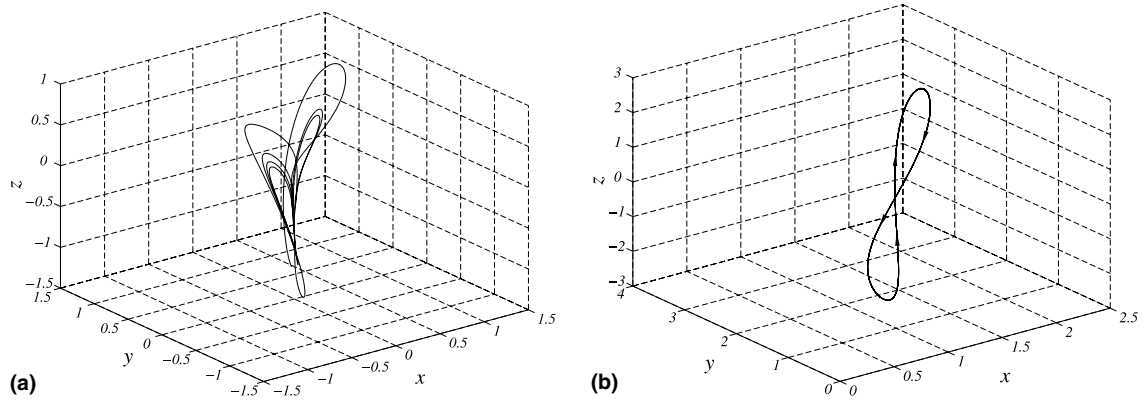

Fig. 6. Known wall temperature: attractor in phase space: (a) $\alpha = 0°$, $\epsilon = 0.05$; (b) $\alpha = 45°$, $\epsilon = 0.05$.

Substituting in the energy equation, and following a similar process as before for the expanded differential equations, with weights $\cos n\theta$ and $\sin n\theta$, we get the three integrals

$$\frac{dT_0'}{dt} = \frac{2}{\pi d^2 \rho c}\left[-\pi dh T_0' + dh\sum_{n=1}^{\infty} T_n^{\mathrm{s}} \frac{(-1)^n - 1}{n} + \widehat{q}\right], \tag{28}$$

$$\frac{\mathrm{d}T_m^{\mathrm{c}}}{\mathrm{d}t} + m\frac{u}{R}T_m^{\mathrm{s}} = \frac{2}{\pi d^2 \rho c}\left[-\pi dh T_m^{\mathrm{c}} + 2dh\sum_{\substack{n=1\\ n\neq m}}^{\infty} nT_n^{\mathrm{s}} \frac{(-1)^{n+m} - 1}{n^2 - m^2}\right], \tag{29}$$

$$\frac{\mathrm{d}T_m^{\mathrm{s}}}{\mathrm{d}t} - m\frac{u}{R}T_m^{\mathrm{c}} = \frac{2}{\pi d^2 \rho c}\left[2dh T_0' \frac{(-1)^m - 1}{m} - \pi dh T_m^{\mathrm{s}} + 2dh\sum_{\substack{n=1\\ n\neq m}}^{\infty} mT_n^{\mathrm{c}} \frac{(-1)^{n+m} - 1}{m^2 - n^2} + 2\widehat{q}\frac{(-1)^m - 1}{m}\right], \tag{30}$$

where $m = 1, 2, \ldots, 2(k+1), \ldots$ and where we have written $T_0' = T_0 - T_{\mathrm{c}}$. The nondimensional equations of the resulting infinite-dimensional dynamical system are

$$\frac{\mathrm{d}x}{\mathrm{d}\tau} = -x + y_1 \cos\alpha - z_1 \sin\alpha, \tag{31}$$

$$\frac{\mathrm{d}y_0}{\mathrm{d}\tau} = \frac{Q}{2} - \frac{H}{2}y_0 + \frac{H}{2\pi}\left[\sum_{n=1}^{\infty} z_n \frac{(-1)^n - 1}{n}\right], \tag{32}$$

$$\frac{\mathrm{d}y_m}{\mathrm{d}\tau} = -\frac{H}{2}y_m + \frac{H}{\pi}\left[\sum_{\substack{n=1\\ n\neq m}}^{\infty} nz_n \frac{(-1)^{n+m} - 1}{n^2 - m^2}\right] - mxz_m, \tag{33}$$

$$\frac{\mathrm{d}z_m}{\mathrm{d}\tau} = -\frac{H}{2}z_m + \frac{Q}{\pi}\frac{(-1)^m - 1}{m} + \frac{H}{\pi}y_0\frac{(-1)^m - 1}{m} + \frac{H}{\pi}\left[\sum_{\substack{n=1\\ n\neq m}}^{\infty} my_n \frac{(-1)^{n+m} - 1}{m^2 - n^2}\right] + mxy_m, \tag{34}$$

where H and Q are the same as in Eqs. (23) and (12).

5.2. Steady states and linear stability

The critical points of the dynamical system are found by first solving the steady-state versions of Eqs. (1), (2) and (27) in dimensional form as

$$\overline{u}^2 = \frac{\widehat{q}\beta g R}{\pi^2 dcf}\left[\cos\alpha. + \frac{2\pi Rh[\cos\alpha + (4Rh/d\rho c\overline{u})\sin\alpha]}{d\rho c\overline{u}[1 + (4Rh/d\rho c\overline{u})^2]} \times \coth\frac{2\pi Rh}{\rho dc\overline{u}}\right], \tag{35}$$

$$\overline{T}(\theta) = \begin{cases} T_{\mathrm{c}} + \dfrac{4R\widehat{q}}{d^2\rho c\overline{u}}\dfrac{\exp\{-4Rh\theta/d\rho c\overline{u}\}}{1 - \exp\{-4\pi Rh/d\rho c\overline{u}\}} \\ \quad \text{for } 0 \leqslant \theta \leqslant \pi, \\ T_{\mathrm{c}} + \frac{4R\widehat{q}}{d^2\rho c\overline{u}}\left[\dfrac{\theta}{\pi} + \dfrac{2\exp\{-4\pi Rh/d\rho c\overline{u}\} - 1}{1 - \exp\{-4\pi Rh/d\rho c\overline{u}\}}\right] \\ \quad \text{for } \pi < \theta < 2\pi. \end{cases} \tag{36}$$

Using the expansion (3) in the above, the Fourier coefficients $\overline{T}_m^{\mathrm{c}}$ and $\overline{T}_m^{\mathrm{s}}$ can be introduced. Nondimensionalization then gives the critical points of Eqs. (31)–(34) as solutions of

$$\overline{x}^2 = Q\left[\frac{2}{\pi}\cos\alpha + \frac{H}{\overline{x}}\left(\frac{\cos\alpha + (H/\overline{x})\sin\alpha}{1 + (H/\overline{x})^2}\right)\coth\frac{\pi H}{2\overline{x}}\right], \tag{37}$$

$$\overline{y}_0 = \frac{Q}{2}\left[\frac{1}{H} + \frac{\pi}{\overline{x}}\left(\frac{3}{2} + \frac{2\mathrm{e}^{-\pi H/\overline{x}} - 1}{1 - \mathrm{e}^{-\pi H/\overline{x}}}\right)\right], \tag{38}$$

$$\overline{y}_m = \frac{Q}{\overline{x}}\left[\frac{H}{\overline{x}[m^2 + (H/\overline{x})^2]}\frac{1 - \mathrm{e}^{-\pi H/\overline{x}}(-1)^m}{1 - \mathrm{e}^{-\pi H/\overline{x}}} + \frac{1 - (-1)^m}{\pi m^2}\right], \tag{39}$$

$$\overline{z}_m = -\frac{QH^2}{m\overline{x}^3[m^2 + (H/\overline{x})^2]}\frac{1 - \mathrm{e}^{-\pi H/\overline{x}}(-1)^m}{1 - \mathrm{e}^{-\pi H/\overline{x}}}, \tag{40}$$

where $m = 1, 2, \ldots$ These steady-state solutions of the fluid velocity and temperature fields were determined by Greif et al. [17] for zero angle of inclination, and by Sen et al. [18] for an inclined thermosyphon.

The steady-state velocity solutions, determined from Eq. (37), are presented in Fig. 7 as $\overline{x}$ vs. α for $H = 0.1$

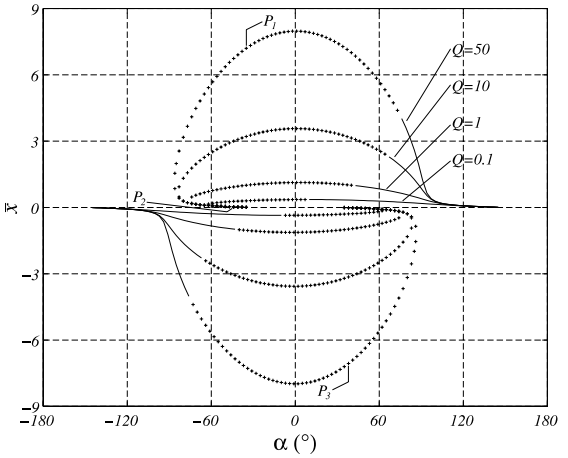

Fig. 7. Mixed conditions: steady-states $\overline{x}(\alpha)$; $H = 0.1$ and different values of Q; − stable; + unstable.

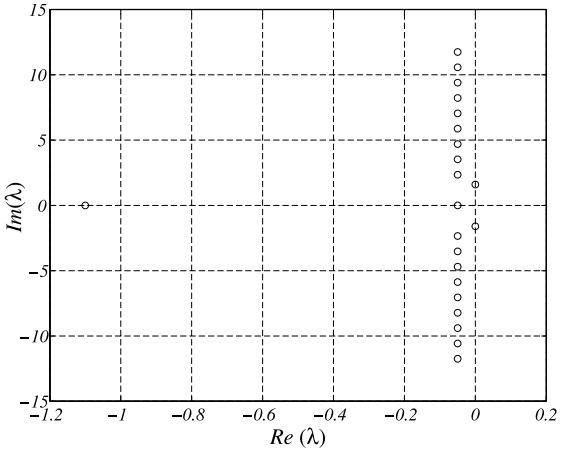

Fig. 8. Mixed conditions: eigenvalues of P_1 for $m = 10$, $\alpha = 45°$, $Q = Q_{cr}$.

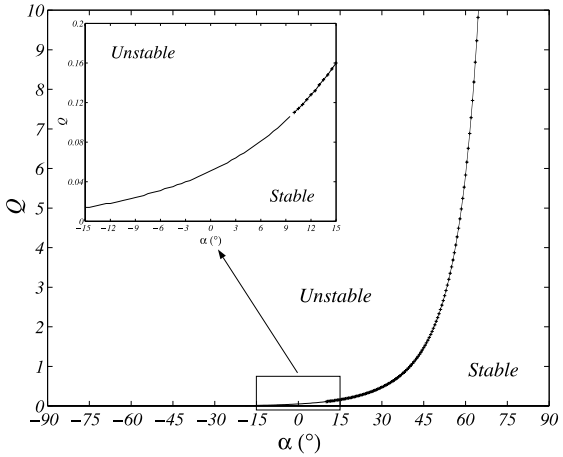

Fig. 9. Mixed conditions: neutral stability curve for P_1 in (Q, α) space. − subcritical; − + − supercritical.

and different values of Q. No critical points exist for $-180° < \alpha < -147.5°$ and $147.5° < \alpha < 180°$; one exists for $-147.5° < \alpha < -\alpha^*$ and $\alpha^* < \alpha < 147.5°$ where α^* varies from $\alpha^* = 32.5°$ when $Q = 0^+$ to $\alpha^* = 90°$ as $Q \to +\infty$; two critical points exist for $-32.5° < \alpha < 32.5°$; and three for $-\alpha^* < \alpha < -32.5°$ and $32.5° < \alpha$

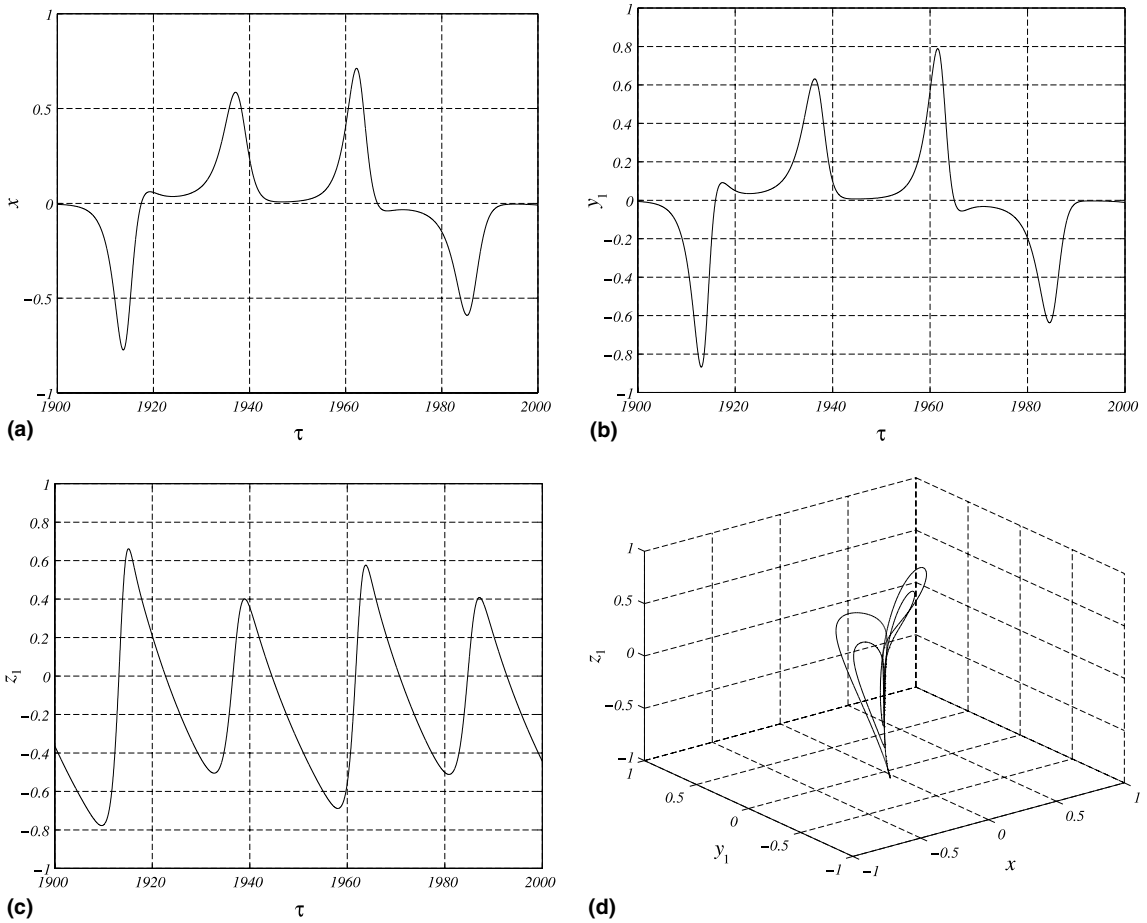

Fig. 10. Mixed conditions: time series (a) $x(\tau)$, (b) $y_1(\tau)$, (c) $z_1(\tau)$, and (d) attractor in phase space for $\alpha = 0°$, $\epsilon = 0.05$.

$< \alpha^*$. The critical points are designated P_1, P_2 and P_3 as before being the outer positive, the inner, and the outer negative branches, respectively.

From a linear stability analysis of the dynamical system the eigenvalues are obtained numerically. To compute the infinite-dimensional system, we truncate the dynamical system up to order m and make sure that m is large enough so that the leading eigenvalues are converged. For $m \geqslant 10$ not only the leading eigenvalues have already converged to their appropriate values but the rest of them as well. In fact, as we increase m new complex conjugate eigenvalues appear with larger imaginary parts but with the same real parts, as shown in Fig. 8 for $m = 10$. This figure shows a typical eigenspectrum for a system of size $2(m+1) = 22$ for $\alpha = 45°$ and $Q = Q_{cr}$, and is qualitatively similar to that on any point along the neutral stability curve. It is interesting to note that, other than the leading eigenvalues and those lying in the real axis, the rest of them are equally spaced. This behavior comes from the nature of the dynamical system itself; why this is so is a detail that is examined in Appendix B.

Once again instability is through imaginary eigenvalues indicating a Hopf bifurcation. The neutral stability curve, Q vs. α with $H = 0.1$, for P_1 is presented in Fig. 9. The stability curve for P_3 is a mirror image with respect to the ordinate. Stable and unstable steady states are also indicated in Fig. 7; P_2 is always unstable. Once again, as the tilt angle increases, higher heat fluxes can be sustained before the steady state loses stability.

5.3. Nonlinear analysis

Solutions of the infinite-dimensional system (31)–(34) can be reduced to trajectories on the two-dimensional center manifold whose projected equations contain the long-time dynamics of the original system. Applications of CMP to infinite systems can be found in Carr [13], Ho and Chang [19], and Chen and Chang [20], among others. After the CMP procedure and normal form analysis, the corresponding Stuart–Landau and phase equations for $Q = (1+\epsilon)Q_{cr}$ are obtained, where Q_{cr} is the critical value. As in the *known wall temperature* case, the results of this analysis show that there is a change

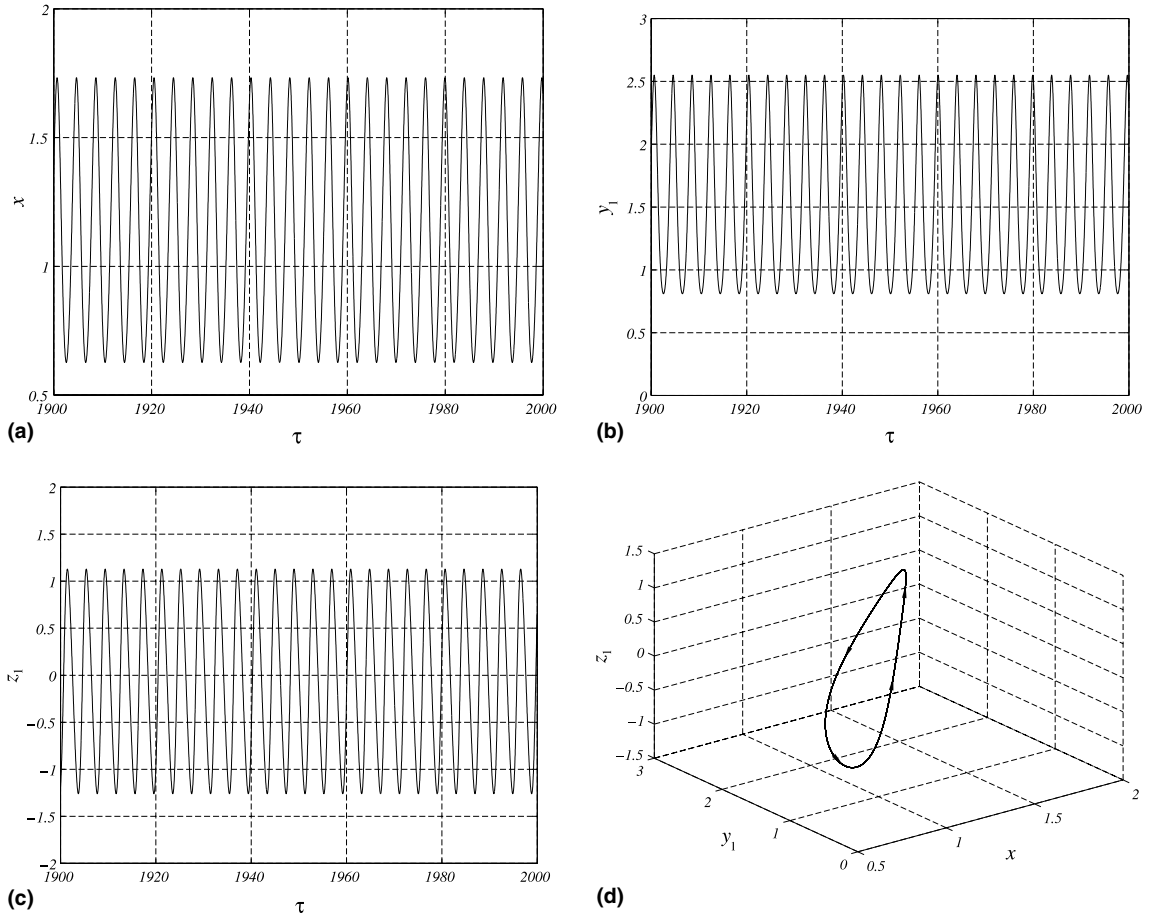

Fig. 11. Mixed conditions: time series (a) $x(\tau)$, (b) $y_1(\tau)$, (c) $z_1(\tau)$, and (d) attractor in phase space for $\alpha = 45°$, $\epsilon = 0.05$.

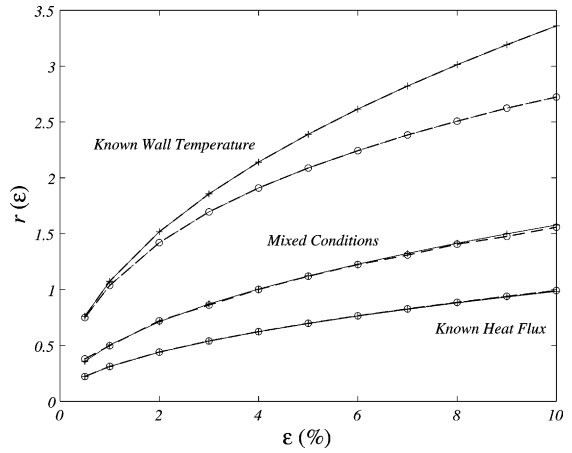

Fig. 12. Comparison between analytically and numerically determined amplitudes for all three heating conditions; $-+-$ analytical; $-\circ-$ numerical.

from sub- to super-criticality of the Hopf bifurcation as one moves along the curve. This is indicated in Fig. 9.

For verification, numerical integration is carried out with $\epsilon = 0.05$ for $\alpha = 0°$ and $\alpha = 45°$. For $\alpha = 0°$ the results are depicted as time dependence and a three-dimensional projection in Fig. 10. Subcriticality is indicated by the appearance of complex trajectories. On the other hand, the corresponding results for $\alpha = 45°$, shown in Fig. 11, indicate periodic limit-cycle behavior since the bifurcation there is supercritical. Comparison of the amplitude of oscillations using the analytical and numerical methods is shown in Fig. 12. Agreement is good and the rms difference between them is less than 2.1%.

The results here qualitatively confirm the chaotic behavior found in the mixed heating experiments of Creveling et al. [5] and Gorman et al. [21] for $\alpha = 0$ which happens to be in the subcritical region. For $-6° < \alpha < 6°$, Damerell and Schoenhals [6] also experimentally found chaotic behavior of the flow.

6. Discussion

This contribution covers three aspects of the toroidal thermosyphon problem: (a) all three heating cases are nondimensionalized in a similar way to be able to compare the results, (b) all three cases include the effect of angular inclinations, and (c) similar nonlinear analyses are carried out for each case. The results show that the selection of a thermosyphon model affects the behavior of the resulting dynamical system, especially in terms of the possible presence or absence of oscillatory behavior, something that is important to know from the point of view of applications. For known heat flux, stable limit cycles always exist, while for the other two cases it is conditional. For mixed conditions at loss of stability, for instance, there is either oscillatory behavior or not depending on parameter values. Truncation of the system, Eqs. (31)–(34), to three equations produces the Lorenz equations for which it is known that the steady state gives way directly to chaos without stable limit cycles.

The results thus show that experimental observations must be compared to the predictions of the appropriate theoretical model. The presence or absence of oscillatory behavior is one aspect that may be different. Furthermore, as shown in Fig. 12, even for parameter values for which there are limit cycles, the amplitudes are different for the same ϵ. If, however, it is intended to show the existence of chaos, then it does not make much difference which model is used.

7. Conclusions

Natural circulation loops have a broad range of applications since they work as dependable heat pumps that do not require external pumps. An adequate knowledge of their operation is necessary for design since the behavior of the system changes with heating values and inclinations. In the present work we have developed analytical models of tilted toroidal thermosyphons for three different heating conditions, and determined their linear and nonlinear characteristics for parameters corresponding to the heat rate and inclination angle. Under known heat flux and known wall temperature conditions the governing equations lend themselves to exact decoupling, while this is not the case for mixed heating where the equations remain coupled as an infinite set.

The center manifold theory and normal form analysis are powerful tools in the study of nonlinear dynamical systems. Here they are applied to finite- and infinite-dimensional dynamical systems to achieve a reduction of the dimension of the dynamical system near a bifurcation point that contains the original behavior. Using this approach we have shown that the solutions for the known heat flux mode bifurcate supercritically along the Hopf curve, while for known wall temperature and mixed heating they can be sub- or super-critical. This may be important in the design of natural convection loops. Numerical experiments have confirmed the theoretical predictions. Generally speaking, the behavior goes from sub- to supercritical as the tilt angle is increased. It must be remembered that the present analysis is only valid in the vicinity of the neutral stability curve. Farther away an increase in the heating parameter always induces chaotic behavior [15].

It is also shown that the orientation of the loop with respect to the gravity vector has a great influence on the linear and nonlinear characteristics of the resulting dynamical system. For all three heating conditions studied, the tilt angle is a stabilizing parameter while the heat rate is a natural destabilizer. In general, the fluid can

reach higher velocities before losing stability as the angle of inclination increases thus advecting larger heat rates. Side heating as opposed to bottom heating may thus be recommended for certain applications.

Acknowledgements

A.P.-V. is the recipient of a CONACyT-Fulbright Fellowship from México for which we are grateful. We also thank the Universidad Nacional Autónoma de México for a DGAPA Scholarship granted to W.F.

Appendix A

We apply the center manifold projection and normal form analysis to the local form, with respect to the critical point P^+, of system (9)–(11) given by

$$\begin{aligned}\frac{dx'}{d\tau} &= -x' + y'\cos\alpha - z'\sin\alpha,\\ \frac{dy'}{d\tau} &= -\sqrt{Q\cos\alpha}\,z' - x'z',\\ \frac{dz'}{d\tau} &= \sqrt{Q/\cos\alpha}\,x' + \sqrt{Q\cos\alpha}\,y' + x'y',\end{aligned} \tag{A.1}$$

where the primes denote deviations from P^+. We now introduce a small perturbation in parameter space of the form $Q_p = \epsilon Q_{cr}$, where $Q_p \sim O(\epsilon)$ and Q_{cr} is the critical value of Q. By applying a similarity transformation, $[x', y', z']^T = \mathbf{T}[w_1, w_2, w_3]^T$, where $\mathbf{T}$ is given by

$$\mathbf{T} = \frac{1}{\cos^2\alpha - 2}\begin{bmatrix} -\sin^2\alpha & \frac{\sqrt{2}}{4}\sin 2\alpha & -1\\ -\sin\alpha\tan\alpha & \frac{\sqrt{2}}{4}\sin\alpha & \sin\alpha\tan\alpha\\ -\sin\alpha & -\sqrt{2}\sin^2\alpha & \sin\alpha\end{bmatrix} \tag{A.2}$$

to the perturbed version of the dynamical system (A.1), we obtain

$$\frac{d\mathbf{w}}{dt} = \Lambda\mathbf{w} + \hat{\mathbf{P}}\mathbf{w} + \mathbf{N}(\mathbf{w}), \tag{A.3}$$

where $\hat{\mathbf{P}}$ is the linear perturbation matrix containing terms of order ϵ, $\mathbf{N}(\mathbf{w})$ are the quadratic nonlinear terms, and Λ is the Jacobian of (A.1) being cast into a Jordan form as

$$\Lambda = \begin{pmatrix} 0 & -\sqrt{2}\tan\alpha & 0\\ \sqrt{2}\tan\alpha & 0 & 0\\ 0 & 0 & -1\end{pmatrix}. \tag{A.4}$$

In (A.4) the neutral eigenvalues are associated with w_1 and w_2. Hence, if we write (A.3) as

$$\frac{d\mathbf{w}^*}{dt} = \mathbf{N}_a(\mathbf{w}^*, w_3); \qquad \frac{dw_3}{dt} = N_b(\mathbf{w}^*, w_3), \tag{A.5}$$

where $\mathbf{w}^* = (w_1, w_2)$, the center manifold theorem [12–14] then states that the trajectories of the system (A.5) near the local origin can be approximated by the two-dimensional system $d\mathbf{w}^*/dt = \mathbf{N}_a[\mathbf{w}^*, \phi(\mathbf{w}^*)]$ provided that $w_3 = \phi(\mathbf{w}^*)$ is a smooth invariant manifold for dw_3/dt in (A.5), and $\phi(0) = D\phi(0)/D\mathbf{w}^* = 0$.

We first focus our attention on the transformation at the Hopf bifurcation point $\epsilon = 0$ which removes $\hat{\mathbf{P}}$ from Eq. (A.3), and approximate a center manifold $\phi(\mathbf{w}^*)$ of the form

$$\phi(w_1, w_2) = c_1 w_1^2 + c_2 w_1 w_2 + c_3 w_2^2 + O(|\mathbf{w}^*|^3) \tag{A.6}$$

since the system (A.3) has only quadratic nonlinearities. On using the chain rule in dw_3/dt of (A.5), with $w_3 = \phi(w_1, w_2)$, and equating powers of w_1^2, $w_1 w_2$ and w_2^2, we find

$$c_1 = -c_3 = k_1 - \sqrt{2}\tan\alpha\, c_2, \quad c_2 = \frac{k_2 + 4\sqrt{2}\tan\alpha\, k_1}{8\tan^2\alpha + 1},$$
$$k_1 = \frac{\sin^2\alpha\sin 2\alpha}{2(\cos^2\alpha - 2)^2}, \quad k_2 = \frac{\sqrt{2}(2 - 3\cos^2\alpha)\sin^2\alpha}{6(\cos^2\alpha - 2)^2}.$$

The reduced system containing the projected equations for the center manifold is given by

$$\frac{dw_1}{dt} = -\sqrt{2}\tan\alpha\, w_2 + s_1(w_1, w_2) + O(|w_1|^4, |w_2|^4), \tag{A.7}$$

$$\frac{dw_2}{dt} = \sqrt{2}\tan\alpha\, w_1 + s_2(w_1, w_2) + O(|w_1|^4, |w_2|^4), \tag{A.8}$$

where s_1 and s_2 include quadratic and cubic nonlinear terms, not shown explicitly due to lack of space. A normal form analysis provides further simplification using a smooth nonlinear coordinate mapping of the type $\mathbf{w}^* = \mathbf{v} + \mathbf{\Psi}(\mathbf{v})$ to transform away many nonlinear terms without losing relevant information. $\mathbf{\Psi}(\mathbf{v})$ is a homogeneous function of $\mathbf{v}$ which can be Taylor expanded. For the present case $\mathbf{\Psi}$ is a polynomial of degree 2 and higher whose coefficients are to be determined. The computation of these terms, for the Hopf bifurcation, are well documented in the literature [14]. Hence, the system (A.7) and (A.8) can be transformed to

$$\frac{d\mathbf{v}}{dt} = \begin{pmatrix} 0 & -\sqrt{2}\tan\alpha\\ \sqrt{2}\tan\alpha & 0\end{pmatrix}\mathbf{v} + \begin{pmatrix} (\sigma v_1 - \gamma v_2)(v_1^2 + v_2^2)\\ (\gamma v_1 + \sigma v_2)(v_1^2 + v_2^2)\end{pmatrix} \tag{A.9}$$

for suitable constants σ and γ which depend on the nonlinear part of (A.7) and (A.8). The type of the bifurcation depends on the sign of σ: positive means subcritical and negative supercritical.

The perturbed version, for small ϵ, of (A.7) and (A.8) is given without explicit construction by

$$\frac{d\mathbf{w}^*}{dt} = \mathbf{A}_{\Lambda}\mathbf{w}^* + \mathbf{A}_{\hat{\mathbf{P}}}\mathbf{w}^* + \mathbf{s}(\mathbf{w}^*), \tag{A.10}$$

where $\mathbf{A}_{\Lambda}$ is the reduced Jacobian of (A.4) associated with w_1 and w_2, and the relevant coefficients in $\mathbf{A}_{\hat{\mathbf{P}}}$ are given later. It is to be noted that the CMP, being a nonlinear map of order $O(|\mathbf{w}^*|^2)$, does not alter the linear part of Eq. (A.3) [19]. Thus, we can transform the linear part of (A.10) to a suitable form without disturbing the nonlinear portion, converted already to the desired normal form (A.9) for $\epsilon = 0$, by means of a near identity linear mapping $\mathbf{v} = \mathbf{u} + \mathbf{B}(\epsilon)\mathbf{u}$ where $\mathbf{B} \sim O(\epsilon)$, which vanishes as $\epsilon \to 0$. For a Hopf bifurcation the linear part of a perturbed Jacobian, $\Lambda + \hat{\mathbf{P}}$, can always be transformed to

$$\begin{aligned}\mathbf{A}_{\delta} &= \begin{pmatrix} \delta(\epsilon) & -\sqrt{2}\tan\alpha \\ \sqrt{2}\tan\alpha & \delta(\epsilon) \end{pmatrix} \\ &= (\mathbf{A}_{\Lambda} + \mathbf{A}_{\Lambda}\mathbf{B} - \mathbf{B}\mathbf{A}_{\Lambda} + \mathbf{A}_{\hat{\mathbf{P}}}),\end{aligned} \tag{A.11}$$

where it is clear that $\delta \sim O(\epsilon)$ so that, to leading order, $\mathbf{A}_{\hat{\mathbf{P}}}$ does not change the coefficients of the leading order nonlinear terms of the transformed equation (A.9). A particular transformation $\mathbf{B}$ with the relevant coefficients of the perturbation matrix $\mathbf{A}_{\hat{\mathbf{P}}}$, necessary to calculate δ, are

$$\begin{aligned}\mathbf{B} &= \begin{pmatrix} 0 & -\frac{\sin 2\alpha}{16\sqrt{2}(\cos^2\alpha - 2)} \\ -\frac{\sin 2\alpha}{16\sqrt{2}(\cos^2\alpha - 2)} & 0 \end{pmatrix}; \\ \mathbf{A}_{\hat{\mathbf{P}}} &= \begin{pmatrix} -\frac{\sin^2\alpha\ \epsilon}{2(\cos^2\alpha - 2)} & \hat{P}_{12} \\ \hat{P}_{21} & 0 \end{pmatrix}\end{aligned} \tag{A.12}$$

from which the value of $\delta(\epsilon)$, given in Eq. (14), was determined. Thus, the complete mapping for the system (A.10) to a normal form is $\mathbf{w}^* = \mathbf{u} + \mathbf{B}(\epsilon)\,\mathbf{u} + \Psi(\mathbf{u})$ so that (A.10) becomes

$$\begin{aligned}\frac{d\mathbf{u}}{dt} &= \begin{pmatrix} \delta(\epsilon) & -\sqrt{2}\tan\alpha \\ \sqrt{2}\tan\alpha & \delta(\epsilon) \end{pmatrix}\mathbf{u} \\ &\quad + \begin{pmatrix} (\sigma u_1 - \gamma u_2)(u_1^2 + u_2^2) \\ (\gamma u_1 + \sigma u_2)(u_1^2 + u_2^2) \end{pmatrix}\end{aligned} \tag{A.13}$$

which is the unfolding for the perturbed Hopf bifurcation. A cylindrical mapping $u_1 = re^{i\theta}$, $u_2 = re^{-i\theta}$ of (A.13) leads us to Eq. (13), where γ appears only in the higher order terms of the phase equation $d\theta/dt$. As indicated before, the Taylor coefficients of $\mathbf{s}$ in Eq. (A.10) are related to σ [14] which is given explicitly in Eq. (14).

Appendix B

From the Jacobian of the system (31)–(34) for m and $(m+1)$, which provide systems of dimensions $2(m+1)$ and $2(m+2)$, respectively, we find the relation

$$\mathbf{J}_{2(m+2)} = \left[\begin{array}{c|c} \mathbf{J}_{2(m+1)} & \mathbf{C} \\ \hline \hat{\mathbf{C}} & \mathbf{J}_{2\Delta m} \end{array}\right], \tag{B.1}$$

where $\mathbf{J}_{2\Delta m}$ is a 2×2 matrix that includes the terms arising from the increased system. Since the terms in the matrices $\hat{\mathbf{C}}$ and $\mathbf{C}$ are either zero or very small in magnitude, the characteristic equations of the systems can be closely associated as $\phi_{m+1}(\lambda) \cong \phi_m(\lambda) \cdot \phi_{\Delta m}(\lambda) = 0$ where $\phi_{m+1}(\lambda)$, $\phi_m(\lambda)$ and $\phi_{\Delta m}(\lambda)$ are the determinants $\mathbf{D}_{2(m+2)}$, $\mathbf{D}_{2(m+1)}$, and $\mathbf{D}_{2\Delta m}$, respectively. It is to be noted that $\mathbf{D}_{2\Delta m}$ contains the characteristic polynomial corresponding to new pair of complex eigenvalues while $\mathbf{D}_{2(m+1)}$ and $\mathbf{D}_{2(m+2)}$ are the characteristic polynomials for m and $(m+1)$, respectively. For $m \geqslant 2$ the eigenvalues are related in the following way:

$$\mathrm{Re}(\lambda_{(m+1)}) \cong \mathrm{Re}(\lambda_{(m)}) \cong -\frac{H}{2}, \tag{B.2}$$

$$\pm\mathrm{Im}(\lambda_{(m+1)}) \cong \pm\left(\frac{m+1}{m}\right)\mathrm{Im}(\lambda_{(m)}), \tag{B.3}$$

where $\lambda_{(m+1)}$ corresponds to $(\lambda_{2m+3}, \lambda_{2m+4})$, and $\lambda_{(m)}$ to $(\lambda_{2m+1}, \lambda_{2m+2})$.

References

[1] D. Japikse, Advances in thermosyphon technology, in: T.F. Irvine, J.P. Hartnett (Eds.), Advances in Heat Transfer, vol. 9, Academic Press, New York, 1973, pp. 1–111.

[2] Y. Zvirin, A review of natural circulation loops in pressurized water reactors and other systems, Nucl. Eng. Des. 67 (1981) 203–225.

[3] B. Norton, S.D. Probert, Natural-circulation solar-energy stimulated systems for heating water, Appl. Energy 11 (1982) 167–196.

[4] R. Greif, Natural circulation loops, ASME J. Heat Transfer 110 (1988) 1243–1258.

[5] H.F. Creveling, J.F. de Paz, J.Y. Baladi, R.J. Schoenhals, Stability characteristics of a single-phase free convection loop, J. Fluid Mech. 67 (1975) 65–84 (Part 1).

[6] P.S. Damerell, R.J. Schoenhals, Flow in a toroidal thermosyphon with angular displacement of heated and cooled sections, ASME J. Heat Transfer 101 (1979) 672–676.

[7] M. Gorman, P.J. Widmann, K.A. Robbins, Nonlinear dynamics of a convection loop: a quantitative comparison of experiment with theory, Physica 19D (1986) 255–267.

[8] R. Acosta, M. Sen, E. Ramos, Single-phase natural circulation in a tilted square loop, Wärme- und Stoffübertragung 21 (1987) 269–275.

[9] J.A. Yorke, E.D. Yorke, Chaotic behavior and fluid dynamics, in: H.L. Swinney, J.P. Gollub (Eds.), Topics in Applied Physics, Hydrodynamic Instabilities and the Transition to Turbulence, Springer, Berlin, 1985, pp. 77–95.

[10] M. Sen, C. Treviño, E. Ramos, One-dimensional modeling of thermosyphons with known heat flux, in: J. Menon (Ed.), Trends in Heat, Mass and Momentum Transfer, vol. 2, Council of Scientific Research Integration, Trivandrum, India, 1992, pp. 161–172.
[11] W.V.R. Malkus, Non-periodic convection at high and low Prandtl number, Mémoires Société Royale des Science de Liège 4 (1972) 125–128.
[12] P.J. Holmes, Center manifolds, normal forms and bifurcation of vector fields with application to coupling between periodic and steady motions, Physica 2D (1981) 449–481.
[13] J. Carr, Applications of Centre Manifold Theory, Springer, New York, 1981.
[14] J. Guckenheimer, P. Holmes, Nonlinear Oscillations, Dynamical Systems, and Bifurcations of Vector Fields, Springer, New York, 1983.
[15] M. Sen, E. Ramos, C. Treviño, The toroidal thermosyphon with known heat flux, Int. J. Heat Mass Transfer 28 (1) (1985) 219–233.
[16] T.B. Benjamin, Applications of Leray–Schauder degree theory to problems of hydrodynamic stability, Math. Proc. Camb. Philos. Soc. 79 (1976) 373–392.
[17] R. Greif, Y. Zvirin, A. Mertol, The transient and stability behavior of a natural convection loop, ASME J. Heat Transfer 101 (1979) 684–688.
[18] M. Sen, E. Ramos, C. Treviño, On the steady-state velocity of the inclined toroidal thermosyphon, ASME J. Heat Transfer 107 (1985) 974–977.
[19] K.-L. Ho, H.-C. Chang, On nonlinear doubly-diffusive Marangoni instability, AIChE J. 34 (5) (1988) 705–722.
[20] C.C. Chen, H.-C. Chang, Accelerated disturbance damping of an unknown distributed system by nonlinear feedback, AIChE J. 38 (9) (1992) 1461–1476.
[21] M. Gorman, P.J. Widmann, K.A. Robbins, Chaotic flow regimes in a convection loop, Phys. Rev. Lett. 52 (25) (1984) 2241–2244.